Comparison of various k-ε models and DSM applied to flow around a high-rise building - report on AIJ cooperative project for CFD prediction of wind environment -

A. Mochida[†], Y. Tominaga[‡], S. Murakami[‡†], R. Yoshie[‡‡],
T. Ishihara[‡‡†] and R. Ooka[‡‡‡]

Abstract. Recently, the prediction of wind environment around a building using Computational Fluid Dynamics (CFD) technique comes to be carried out at the practical design stage. However, there have been very few studies which examined the accuracy of CFD prediction of flow around a high-rise building including the velocity distribution at pedestrian level. The working group for CFD prediction of wind environment around building, which consists of researchers from several universities and private companies, was organized in the Architectural Institute of Japan (AIJ) considering such a background. At the first stage of the project, the working group planned to carry out the cross comparison of CFD results of flow around a high rise building by various numerical methods, in order to clarify the major factors which affect prediction accuracy. This paper presents the results of this comparison.

Key words: CFD; wind environment; revised $k\text{-}\varepsilon$ models; Durbin's $k\text{-}\varepsilon$ model.

1. Introduction

The prediction of wind environment around a building using Computational Fluid Dynamics (CFD) technique comes to be carried out at the practical design stage in recent years. For the purpose of this type of prediction, pedestrian level winds should be reproduced with certain accuracy. Recently, the performance of CFD prediction of flow around a bluff body based on various turbulence models has been investigated by many authors. However, there have been very few studies which examine the accuracy of CFD prediction of flow around a high-rise building including the velocity distribution at pedestrian level. The working group* for CFD prediction of wind environment around building, which consists of researchers from several universities and private companies, was organized in the air environment sub-committee in the Architectural Institute of Japan (AIJ) considering such a background.

---

† Associate Professor, Graduate School of Engineering, Tohoku University, 06, Aoba, Sendai, Miyagi, 980-8579, Japan
‡ Associate Professor, Niigata Institute of Technology, 1719, Fujibashi, Kashiwazaki-shi, Niigata, 945-1195, Japan
‡† Professor, Keio University, 3-14-1, Hiyoshi, Kita-ku, Yokohama-shi, Kanagawa, 223-8522, Japan
‡‡ Dr. Engineering, Maeda Corporation, 1576-1, Tsukinowa, Namerikawa, Hiki-gun, Saitama, 355-0313, Japan
‡‡† Associate Professor, Graduate School of Engineering, University of Tokyo, 7-3-1, Hongo, Bunkyo-ku, Tokyo, 113-8656, Japan
‡‡‡ Associate Professor, Institute of Industrial Science, University of Tokyo, 4-6-1, Komaba, Meguro-ku, Tokyo, 153-8505, Japan

At the first stage of the project, the working group planned to carry out the cross comparison of CFD results of flow around a high rise building by various RANS models, i.e., the standard k-ε model, five types of revised k-ε models and Differential Stress Model(DSM), in order to clarify the major factors which affect prediction accuracy. This paper presents the results of this comparison.

2. Outline of the cross comparison

2.1. Flowfield analyzed for this study

The flowfield selected as a test case was the flow around a high-rise building model with the scale ratio of 1:1:2 placed within the surface boundary-layer (cf. Fig.1). For this flowfield, detailed measurements were reported by Ishihara and Hibi (1998). Wind velocity was measured by a split-fibre probe which can discern three-dimensional components of velocity vector (Ishihara *et al*. 1999). This is one of the most reliable data for this kind of flowfield at the present. The Reynolds number based on H (building height) and U_0 (inflow velocity at $z = H$) was 2.4×10^4.

2.2. Computed cases

Outlines of all the computed cases are listed in Table 1. Nine groups have submitted a total of eighteen datasets of results.

2.3. Turbulence models and computational methods

The results based on k-ε models were submitted from many contributors, because k-ε models are still commonly used in practical applications. The performance of the standard k-ε and six types of revised k-ε models was examined. The outline of the revised k-ε models compared here is described in Appendix 1. Unsteady calculations were carried out using the standard and revised k-ε models in MMK1, KE8, LK2, LK2, MMK2, DBN and KE7. But results of these cases showed almost no vortex shedding. Furthermore, DSM (Murakami *et al*. 1993)(cf. Appendix 2) and Direct Numerical Simulation (DNS) with third-order upwind scheme (Kataoka and Mizuno 1999) were also included for a comparison. Results of DSM and DNS reproduced the periodic fluctuations due to vortex shedding.

In order to assess the performance of turbulence models, the results should be compared under the same computational conditions. Special attentions were paid to this point in this study. The computational conditions, i.e., grid arrangements, boundary conditions, etc., were specified by the organizers as described in next section. For the spatial derivatives, QUICK scheme is recommended for all convection terms. From the authors' experience on simulation of flow around a bluff body using k-ε models, no significant difference was observed in applying commonly used numerical
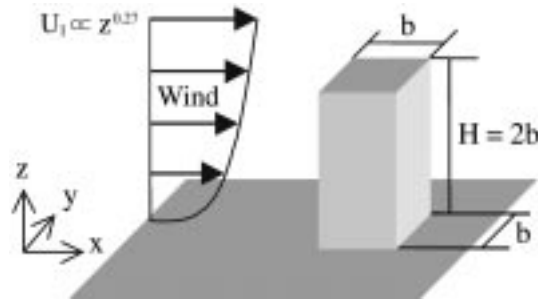
Fig. 1 Flowfield analyzed for this study (Ishihara and Hibi 1998)

Table 1 Computed cases

Affiliation	Software	Turbulence model	Scheme for convection terms	Computational method and time integral scheme	X_R/b	X_F/b	CASE
A	STREAM ver.2.10	k-ε (standard)	QUICK	SIMPLE, steady solution	–	2.54	KE1
B	STREAM ver.2.10	k-ε (standard)	QUICK (1st-order upwind for k and ε)	SIMPLE, steady solution	–	1.66	KE2
C	STREAM ver.2.10	k-ε (standard)	QUICK	SIMPLE, steady solution	–	2.00	KE3
		k-ε (LK)			0.87	2.98	LK1
D	STREAM ver.2.10	k-ε (standard)	QUICK	SIMPLE, steady solution	–	2.00	KE4
		k-ε (RNG)	QUICK		0.50	2.80	RNG1
E	STAR-LT ver.2.0	k-ε (standard)	QUICK	SIMPLE, steady solution	–	2.20	KE5
F	Homemade	k-ε (MMK)	QUICK	MAC, unsteady solution with implicit scheme	0.65	2.72	MMK1
G	FLUENT ver.5.0	k-ε (standard)	Central	SIMPLE, steady solution	–	2.41	KE6
		k-ε (RNG)			0.58	3.34	RNG2
	Homemade	k-ε (standard)	QUICK	HSMAC, unsteady solution with implicit scheme	–	2.70	KE8
		k-ε (LK)			0.58	3.19	LK2
		k-ε (modified LK)			0.53	3.11	LK3
		k-ε (MMK)			0.52	3.09	MMK2
		k-ε (Durbin)			0.63	2.70	DBN
		DSM			>1.0	4.22	DSM
H	Homemade	k-ε (standard)	QUICK	HSMAC, unsteady solution with implicit scheme	–	1.98	KE7
I	Homemade	DNS	3rd-order Upwind	Artificial compressibility method, explicit	0.92	2.05	DNS
Experiment (Ishihara and Hibi 1998)					0.52	1.42	

schemes, QUICK and second-order centered difference, since numerical viscosity generated by the QUICK scheme is generally much smaller than the eddy viscosity v_t predicted by k-ε models in the area flow around a bluff body (Murakami and Mochida 1988, Murakami *et al.* 1990).

3. Preliminary calculations for determining the boundary conditions for the cross comparison (Yoshie 1999)

3.1. Boundary condition for ground surface

3.1.1. Purpose of the preliminary computations

When choosing the ground surface boundary conditions, the most important premise is that the vertical profiles of velocity and turbulent energy at inflow boundary are maintained to the outflow boundary in the computation of a simple boundary layer flow without building. However, calculations conducted so far for the applications of wind environment around buildings do not always adopt appropriate boundary conditions of ground surface which can satisfy this premise. Before doing the cross comparison, two-dimensional computations of the boundary layer flow were conducted at the first stage of this project in order to determine a suitable ground surface boundary conditions used in the cross comparison.

3.1.2. Ground surface boundary conditions compared in this study

Following are the two types of ground surface boundary conditions used for comparison (cf. Table 2) :
(1) Case 1: the logarithmic law for the smooth wall

$$\frac{\langle u_i \rangle_P}{u_*} \;=\; \frac{1}{\kappa}\ln\frac{u_* h_P}{\nu} + 5.5 \tag{1}$$

The value of u_* was derived by the iteration of Eq. (1), using the value of $<u_i>_P$ and h_P, and it was then incorporated into the momentum equation as the wall shear stress $\tau_w = \rho u_*^2$.
(2) Cases 2~5 : the logarithmic law of the form containing the roughness length z_0

$$\frac{\langle u_i \rangle_P}{u_*} \;=\; \frac{1}{\kappa}\ln\!\left(\frac{h_P}{z_0}\right) \tag{2}$$

The value of u_* is obtained by Eq. (2), using the value of $<u_i>_P$, h_P and z_0, and it was implemented into the momentum equation as $\tau_w = \rho u_*^2$ in the same manner as in Case 1. In this type of boundary condition, it is very important to determine the value of z_0 appropriately. In Case 2, the value of z_0 was estimated to be 1.36×10^{-6} m from the velocity gradient near the ground surface at the inflow in the experiment (cf. Fig. 2). For comparison, this value was increased by 10, 100 and 800 times for Cases 3~5.

Table 2 Computed cases for investigating ground surface boundary condition

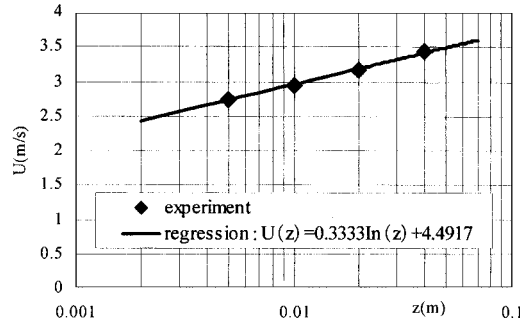| Case	Types of boundary condition	
1	Logarithmic law for smooth wall	
2	Logarithmic law with z_0	$z_0 = 1.36 \times 10^{-6}$ m
3		$z_0 = 1.36 \times 10^{-5}$ m (Case2 $\times$ 10)
4		$z_0 = 1.36 \times 10^{-4}$ m (Case2 $\times$ 100)
5		$z_0 = 1.10 \times 10^{-3}$ m (Case2 $\times$ 800)

Fig. 2 Velocity gradient near the ground in the experiment

3.1.3. Other numerical conditions of the preliminary calculations

(1) Software: STREAM ver.2.10 (Software Cradle Co., Ltd)
(2) Turbulence model : Standard k-ε model
(3) Computational domain : $20b(x_1) \times 7.68b(x_3)$
(4) Grid discretization : $40(x_1) \times 32(x_3)$. The grid width adjacent to ground surface was set at $0.102b(= 0.0082$ m$)$, and the expansion ratio of grid width (grid stretching ratio) in the vertical direction was set at 1.05.
(5) Scheme for convection terms : QUICK scheme
(6) Boundary conditions : At inflow boundary, the interpolated values of velocity and k from the experimental results (Ishihara and Hibi 1998) are imposed. The value of ε was given by Eq. (3) assuming local equilibrium of $P_k = \varepsilon$.

$$\varepsilon \cong P_k \cong -\langle u'w' \rangle \frac{d\langle u \rangle}{dz} \tag{3}$$

$-\langle u'w' \rangle$ and $d\langle u \rangle / dz$ were obtained by interpolating experimental data (Ishihara and Hibi 1998). The velocity gradients normal to the upper and outflow boundaries were assumed to be zero. The normal velocity component defined at the upper boundary was also set to zero.

3.1.4. Results of calculations

Fig. 3 shows the vertical profiles of $<u>$ near the ground surface at positions $5b$ and $10b$ downstream from the inflow boundary. The result of Case 2 ($\times$), which has the smallest z_0 shows the quickest recovery of velocity near the ground surface. On the other hand, the result of Case 5 ($\bullet$)

which has the largest z_0 shows too much decrease of velocity. There are no large differences between Case 1 (the logarithmic law for the smooth wall) and the logarithmic law with small z_0 (Cases 2, 3), and these velocities recovered quickly. The inflow profile was well maintained in Case 4 ($\square$) in comparison with other cases.

As mentioned in 3.1(2), the value of z_0 in Case 2 was obtained from the inflow profile in the experiment. However, the velocity profile in Case 2 shows a large discrepancy from this inflow profile. The reason for this discrepancy can be explained as follows : The velocity gradient near the ground surface shown in Fig. 2 was formed by friction on the wind tunnel floor, but the structure of the entire boundary layer including the velocity gradient at upper height was dominated by the size of roughness in the wind tunnel. Therefore, a larger value of z_0 would be appropriate for maintaining the inflow profile. The order of the z_0 value used in Case 4 (1.36×10^{-4} m; 100 times larger than in Case 2) can be derived by the following process.

If the boundary layer formed near the ground can be regarded as the constant flux layer, the value of u_* can be estimated by the following equation using the value of k at closest point to the ground in the experiment ($z = 0.0625b$),

$$u_* \cong C_\mu^{1/4}\sqrt{k} = 0.09^{1/4}\sqrt{0.37} = 0.33 \mathrm{m/s} \tag{4}$$

Substituting this u_* value and the velocity value at the height $z = 0.0625b$ (2.75 m/s) to Eq. (2), the value of z_0 was calculated to be 1.8×10^{-4}m. The computation with this z_0 value had almost same results as in Case 4.

From the results of these preliminary calculations, we decided to use the logarithmic law of the form containing the z_0 (its value is 1.8×10^{-4} m, $1.125 \times 10^{-3} H$ in normalized value) in the cross comparison presented in section 4.

3.2. Other calculation conditions

3.2.1. Computed cases to investigate the effects of other conditions

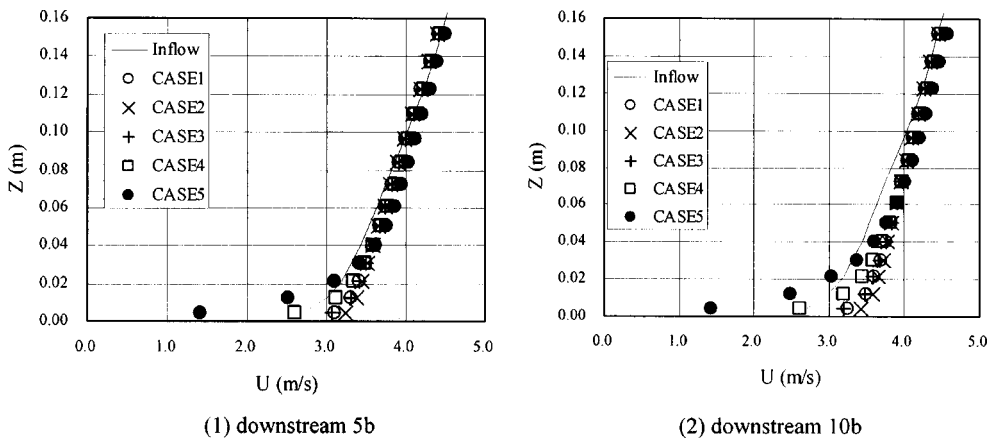The boundary condition for ground surface was determined as described in the previous section.

(1) downstream 5b   (2) downstream 10b

Fig. 3 Vertical profiles of $<u>$ in downstream position (Computations)

Next, it is necessary to decide other calculation conditions, i.e., the computational domain, grid discretization and upper and lateral boundary conditions etc. The basic boundary conditions for the cross comparison were determined as shown in Table 3. The calculations under the basic condition were labelled Case 1 (which corresponds to KE3 in Table 1). Specifications of the computed cases are shown in Table 4. Five cases of computations were conducted with different boundary conditions in order to investigate the effect of other calculation conditions on the results.

(1) Effect of the inflow profile at upper height (Case 2)

In the basic condition, the vertical distributions of the quantities at the inflow boundary were set based on the experimental values (Ishihara and Hibi 1998). The profiles of these values have gradient near the ceiling in the experiment (see Fig. 4). In the region where $z/b > 8.0$ in Case 2, the quantities were set equal to the values at $z/b = 8.0$.

(2) Effect of the size of computational domain (Case 3)

In the basic condition, the length and height of the computational domain were the same as the size of the wind tunnel, and its boundary is treated as solid wall. In Case 3, the computational domain was made smaller, as shown in Fig. 5, and the zero gradient conditions are imposed in upper and lateral boundaries.

(3) Effect of grid discretization (Case 4)

The basic conditions of grid discretization were shown in Fig. 5. In Case 4, the computational

Table 3 Basic conditions for the cross comparison

Computational domain	The computational domain covers $21.5b(x) \times 13.75b(y) \times 11.25b(z)$, which corresponds to the size of wind tunnel
Inflow boundary	The interpolated values of $<u>$ and k from the experimental results are imposed. The vertical profile of mean velocity $<u(z)>$ approximately obeys a power law expressed as $<u(z)> \propto z^{0.27}$ in the experiment. The value of ε is given from the relation $P_k = \varepsilon$.
Lateral and upper surfaces of the computational domain	The wall functions based on logarithmic law for a smooth wall are used.
Downstream boundary	Zero gradient condition is used.
Ground surface boundary	The velocity boundary condition uses a logarithmic law of the form containing the roughness length z_0. The friction velocity u^* is given from the relation $u^* = C_\mu^{1/4} k^{1/2}$ using the experimental values of k, and the value of $1.125 \times 10^{-3}H$ is obtained for z_0 based on this u^* value and the measured velocity profile.
Building surface boundary	The wall functions based on logarithmic law for a smooth wall are used
Grid discretization	The computational domain is discretized into $60(x) \times 45(y) \times 39(z)$ grids. The minimum grid width is $0.07b$ (cf. Fig. 5)
Scheme for convection terms	The QUICK scheme is applied for all convection terms.
Other conditions	The commonly used methods in each affiliation are adopted for the numerical conditions without the specification.

Table 4 Computed cases for investigating other conditions

Case	Computational domain	Grid discretization	Inflow boundary	Sides and upper boundaries
1	Basic	Basic	Basic	Basic
2	Basic	Basic	As shown in Fig. 4	Basic
3	Smaller	Basic	Basic	Zero gradient
4	Smaller	Fine	Basic	Zero gradient
5	Basic	Basic	Eq. (3) for ε	Basic

Fig. 4 Inflow boundary condition for the basic conditions

domain was the same as in Case 3, but the grid resolution was improved. The grid width in Case4 is only one-half to that in Case 3. The grid width adjacent to the building is $b/14$ in horizontal direction in Case 3, while it is reduced to $b/28$ in Case 4.

(4) The effect of the ε values at the inflow boundary

In the basic condition, the ε values at the inflow boundary are given from the following equations which assumed in the relation to $P_k = \varepsilon$:

$$\varepsilon = C_\mu k^{3/2} / l \tag{5}$$

$$l = (C_\mu^{1/2} k)^{1/2} (d<u>/dz)^{-1} \tag{6}$$

In Case 5, Eq. (3) is used to obtain the ε values with $<u'w'>$ derived from the experiment (Ishihara and Hibi 1998).

3.2.2. Results

Fig. 6 shows the vertical distributions of stream-wise velocity $<u>$ behind the building. Case 5 shows slightly smaller velocity value of reverse flow than Case 1. However, the differences in the calculation results for all cases were small. It was confirmed that the result from the computation under the basic conditions are not influenced by the size of computational domain, grid discretization,
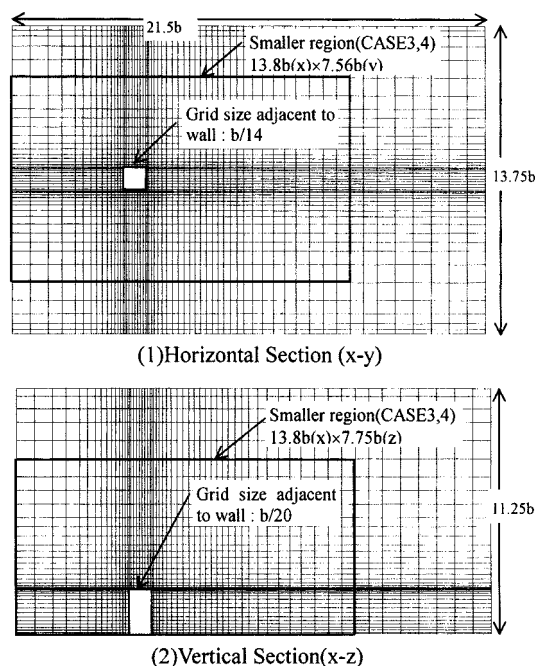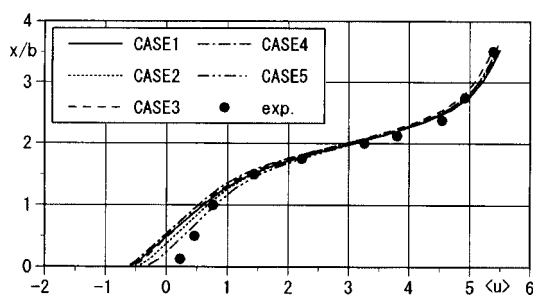
(1)Horizontal Section (x-y)

(2)Vertical Section(x-z)

Fig. 5 Computational domain and grid discretization

Fig. 6 Vertical distributions of $<u>$ behind the building

upper and lateral boundary conditions. Contributors of the cross comparison were requested to follow this basic conditions.

4. Overview of the results of the cross comparison

4.1. Reattachment lengths

The predicted reattachment lengths on the roof, X_R, and that behind the building, X_F, are given for all cases in Table 1. Definition of reattachment lengths X_R and X_F is shown in Fig. 7. In the results of the standard k-ε (KE1~8), the reverse flow on the roof, which is observed in the experiment, is not reproduced as is pointed out in the previous researches by the authors (Murakami *et al.* 1990,
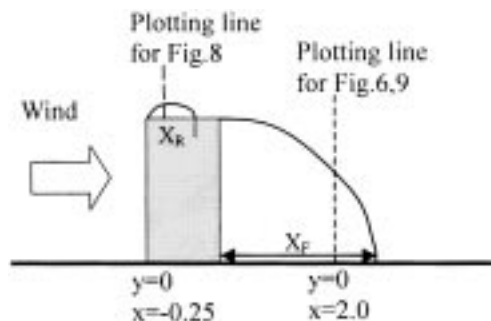
Fig. 7 Definitions of X_R and X_F and position of plotting lines

Murakami 1993). On the other hand, the reverse flow on the roof appears in the results of the revised k-ε models (LK1, RNG1, MMK1, RNG2, LK2, LK3, MMK2, DBN), although its size becomes a little larger than the experiment in the most of these results. In the DSM, the separated flow region from a windward corner is too large, and does not reattach to the roof. DNS with third-order upwind scheme can reproduce the reattachment on the roof, but X_R is overestimated in DNS.

The reattachment length behind the building, X_F, is evaluated larger than the experiment in all cases. It should be noted that the results of the revised k-ε models are in the tendency to evaluate X_F larger than the standard k-ε. DSM greatly overestimates X_F. DNS reproduces fairly well the recirculation flow behind the building. It is surprising to see that there are considerable differences in X_F values between the results of the standard k-ε model. As is already noted, the grid arrangements and boundary conditions were set to be identical in all cases, and QUICK scheme was used for convection terms in many cases. The reason for the difference in X_F values predicted by the standard k-ε model is not entirely clear now, but it may be partly due to the difference in some details of numerical conditions, e.g., the convergence condition, etc..

4.2. Distributions of k on the roof (Fig. 8)

To simplify the comparison, the computed cases were classified into the following four groups based on the software and turbulence model used (cf. Table 1):
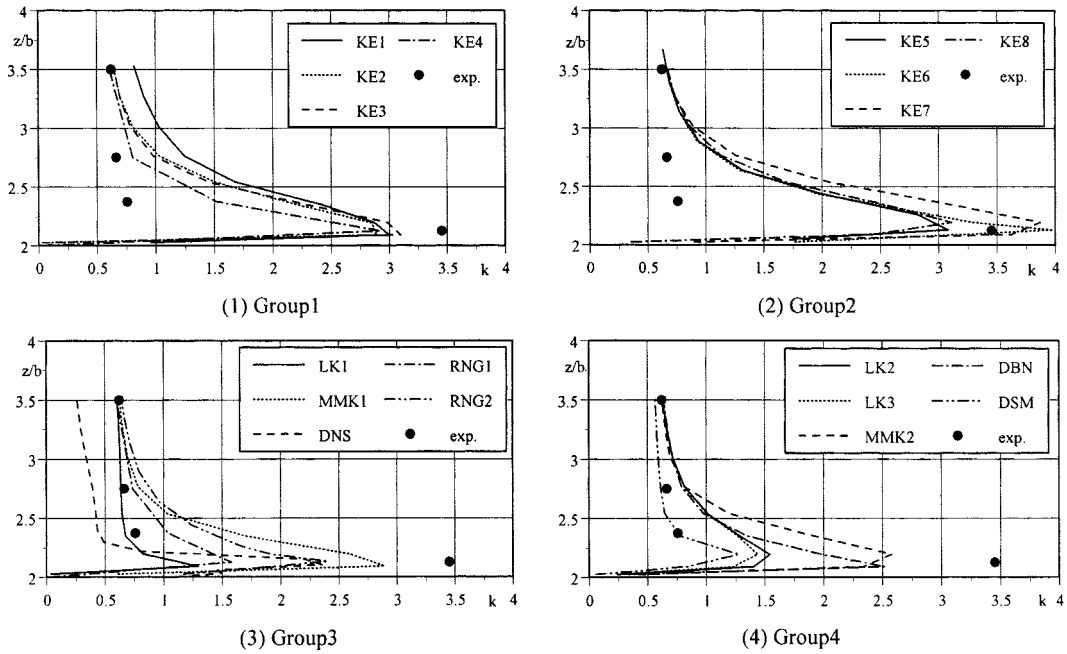
Group 1 : KE1, KE2, KE3, KE4 (the standard k-ε model using 'STREAM')
Group 2 : KE5, KE6, KE7, KE8 (the standard k-ε model using other software)
Group 3 : LK1, MMK1, DNS, RNG1, RNG2 (the modified k-ε models and DNS)
Group 4 : LK2, LK3, MMK2, DBN, DSM (the modified k-ε models and DSM by the affiliation G)

Fig. 8 shows the vertical distributions of k on the roof ($x / b = 0.25$). The plotting line is indicated in Fig. 7. The standard k-ε model greatly overestimates k in the upwind corner of the building as is pointed out in the previous researches by the authors (Murakami *et al.* 1990, Murakami 1993). Therefore, all of the standard k-ε (Groups 1 and 2) showed that the values of k were greater than those of the modified k-ε and other models (Groups 3 and 4) in the area $z / b > 2.5$. Because of this overestimation of k, the reverse flow on the roof was not reproduced in the standard k-ε. On the other hand, the values of k in the modified k-ε and other models evaluated to be slightly smaller

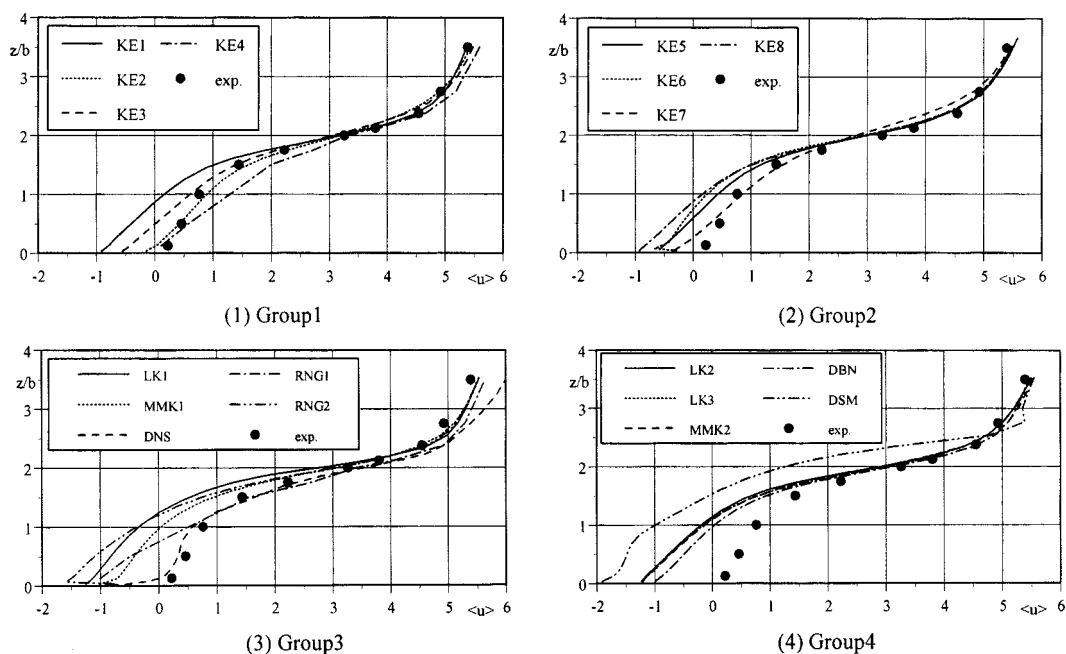Fig. 8 Vertical distributions of *k* on the roof

than that of the experiment at height $z / b = 2.125$. This underestimation of *k* made the reverse flow region on the roof rather large in the modified *k-ε* and other models (cf. Table 1). This tendency was especially noticeable in the DSM of Group 4. The differences in the values of *k* on the roof seem to affect the differences in distribution of *k* and the reattachment lengths behind the building.

4.3. Vertical distributions of <u> behind the Building (Fig. 9)

Fig. 9 shows the vertical distributions of the stream-wise component of velocity $<u>$ behind the building. Above the building height ($z / b = 2.0$), the values of all of the models correspond well with the experimental values. However, there are large differences among cases near the ground surface ($z / b < 1.0$) corresponding to the difference in the reattachment length, X_F. In this region, the velocity in the reverse flow of the modified *k-ε* and other models (Groups 3 and 4) showed larger negative values than the standard *k-ε* (Groups 1 and 2). The most accurate information on velocity in this region was obtained by the DNS of Group 3.

4.4. Scalar velocity distributions near the ground surface (Fig. 10)

The horizontal distributions of scalar velocity near ground surface ($z = 0.0625H = 1/16H$) is compared in Fig. 10. These values are normalized by the velocity value at the same height at inflow boundary. As shown in Fig. 10, the almost similar results are obtained by standard *k-ε* and modified models. However, some characteristic flow patterns peculiar to each software used by each affiliation are observed. Hence there exist some differences between the results according to the difference in the software used in each case. When we compare the results between the standard and modified *k-ε*

Fig. 9 Vertical distributions of $<u>$ behind building

models predicted by the same software (for example, KE3 vs. LK1 or KE8 vs. LK2, LK3, MMK2, and DBN), the modified k-ε models tend to show a slightly wider region where the normalized velocity value exceeds 1.2 at the sides of the building. This region is extremely wide in DSM and DNS.

4.5. Applicability of the Durbin's modified k-ε model

As previously mentioned, every modified k-ε models and DSM could reproduce the reverse flow on the roof, which does not appear in the results of the standard k-ε model. On the other hand, most modified k-ε models overestimated the reattachment length behind the building in comparison with the standard k-ε model. This tendency is also reported in the computation for the flowfield around a cube placed on channel wall by Lakehal and Rodi (Lakehal and Rodi 1997).

In order to investigate the performance of turbulence model in the same condition, we select the results given from the homemade software by the affiliation G, i.e., the standard k-ε (KE8), the LK models (LK2, LK3), MMK model (MMK2), Durbin's model (DBN) and DSM (cf. Appendix 1, 2). As is shown in Table 1, the X_F of the Durbin's model (DBN) is the same as that of the standard k-ε model (KE8), although other RANS models (LK2, LK3, MMK2 and DSM) have larger X_F in comparison with KE8. According to this, as shown in Fig. 9, the vertical distribution of $<u>$ behind building of Durbins' model (DBN in Group 4) is very close to that of the standard k-ε (KE8 in Group 2), which shows better agreement with the measured values.

As shown in Fig. 10, rather similar results of the horizontal distribution of scalar velocity near ground surface are obtained by the selected cases ((9), (15)~(19) in Fig. 10). However, the area where normalized velocity value exceeds 1.4 becomes wider in DBN than those of other models.
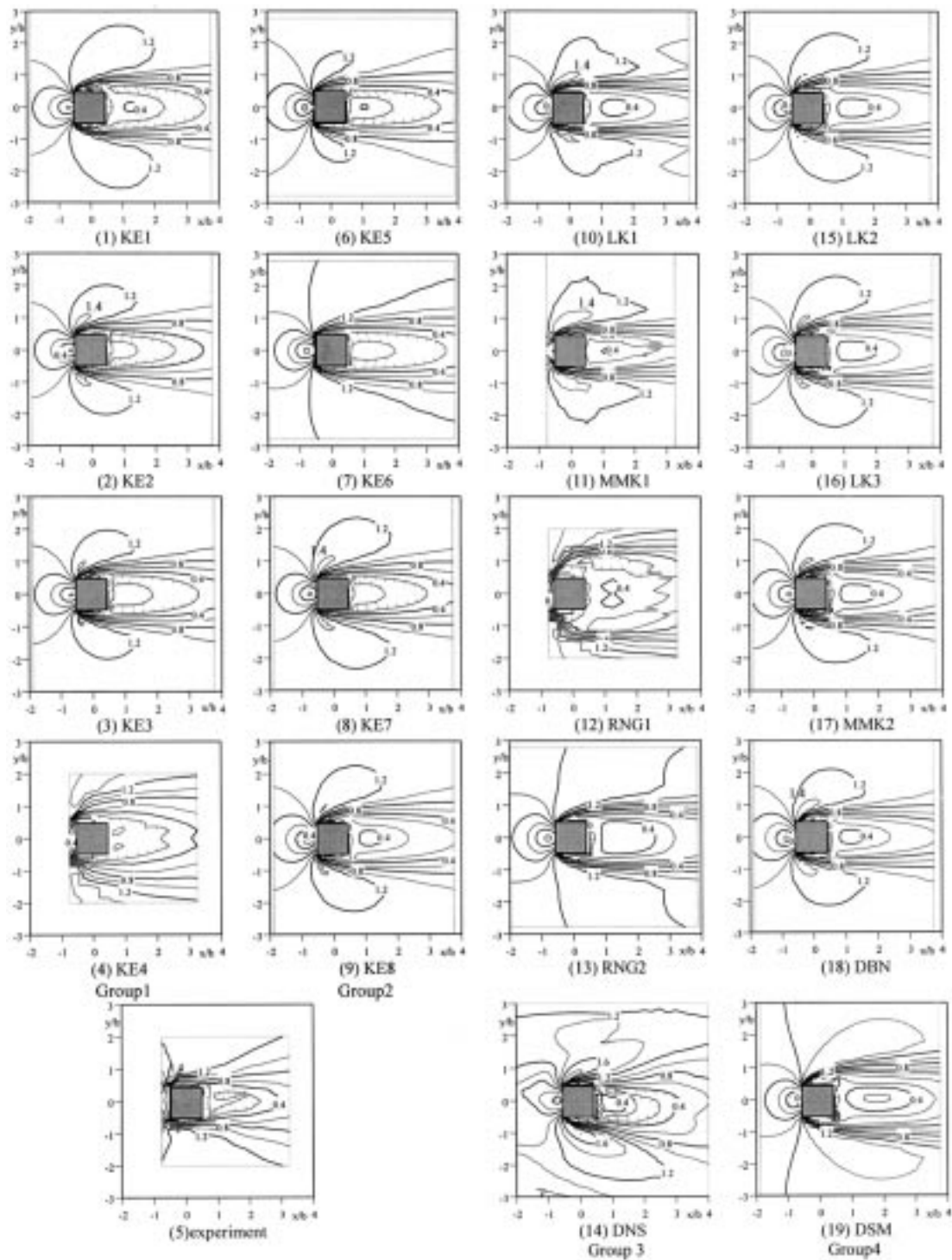
Fig. 10 Horizontal distributions of scalar velocity at $z = 1/16H$ height (Values are normalized by the velocity value at the same height at inflow boundary)
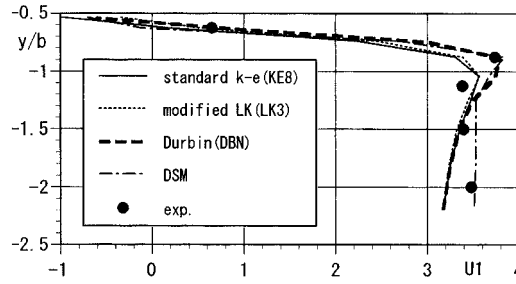
Fig. 11 Horizontal distributions of $<u>$ along lateral direction (y) near ground surface ($z = 1/16H$)

DSM greatly overestimates the velocity increase near the corner due to the separation.

Fig. 11 shows the horizontal distributions of $<u>$ along the lateral direction near the ground surface in the area affected by the separation at the frontal corner in the selected cases. The peak in the measured velocity distribution appears at $y/b = -0.9$. The standard k-ε (KE8) and the modified LK model (LK3) underestimate the velocity value around this point. As for the Durbin's model (DBN), the position and the peak value in the velocity distribution are well reproduced. In DSM, the velocity values are evaluated generally larger in the region $y/b < -1.5$ in comparison with other computations.

Judging from the results compared here, the applicability of the Durbin's modified k-ε model to the flowfield around building seems to be quite good. Fig. 12 illustrates the time scale T calculated by Durbin's model (Eq. (15) in Appendix 1). Around the frontal corner of the roof, the estimated value of T is very small, because the strain rate scale S becomes large. Hence, the value of v_t in Durbin's model is calculated small in comparison with the standard k-ε model. This smaller value of v_t in Durbin's model reproduce the reverse flow on the roof, which does not appear in the standard k-ε model. In the Durbin's model, the value of T derived by the 'realizability', T_D, is utilized only in the region where the value is calculated smaller than that in the standard k-ε model (k/ε ; T_S). Fig. 13 shows the ratio of two time scales (T_D/T_S). The shaded area shown in Fig. 13 indicates the region of $T_D/T_S < 1.0$ where the the Durbin's time scale, T_D, is adopted. This figure means the Durbin's time scale is utilized only around the frontal corner of the roof, that is, the standard
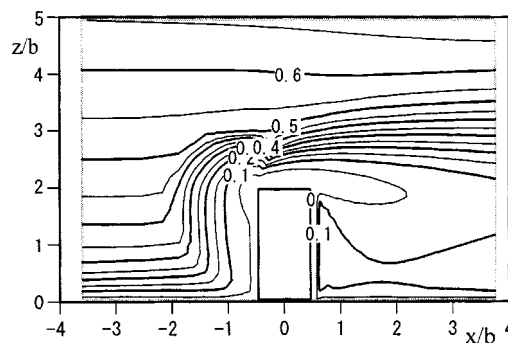

Fig. 12 Vertical distribution of the time scale T (Eq. (15) in Appendix 1) by Durbin's model
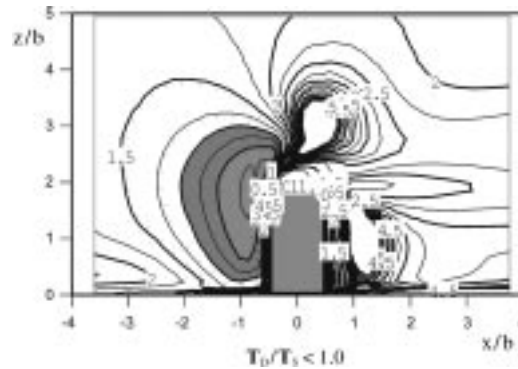
Fig. 13 Ratio of two time scales (T_D / T_S)

k-ε model is applied for other region in Durbin's model. This is the reason that the prediction accuracy of flowfield behind the building in Durbin's model is almost same as that in the standard k-ε model.

5. Conclusions

(1) A suitable boundary conditions for the cross comparison of the flowfield around a high-rise building model placed within the surface boundary-layer were investigated in the preliminary computations. It was confirmed that the velocity profile at inflow boundary can be maintained in the downstream region in the computation using the logarithmic law involving the z_0 if appropriate value of z_0 is given based on the measured velocity and k near the ground surface.

(2) Under the same calculation conditions derived from the preliminary studies, the flowfield around a high-rise building was analyzed using the standard k-ε model, five types of revised k-ε models and DSM. Results of these analyses were compared with experimental data.

(3) Large differences were observed in the prediction results given from the various k-ε models and DSM, in particular in the region near the corner of the building model.

(4) The standard k-ε model could not reproduce the reverse flow on the roof. This drawback was corrected by all revised k-ε models tested here. But most revised k-ε models overestimated the reattachment length behind the building in comparison with the standard k-ε model.

(5) For the flowfield treated in this cross comparison, the result with the model proposed by Durbin showed the best agreement with the experiment among the results given from the revised k-ε models compared here.

Acknowledgements

References

Craft, T. J. and Launder, B. E. (1992), "A new wall of 'wall-reflection' effects on the pressure-strain correlation and its application to the turbulent impinging jet", *AIAA J.*, **30**, 2970-2981.

Durbin, P. A. (1996), "On the k-ε stagnation point anomaly", *Int. J. Heat and Fluid Flow*, **17**, 89-90.

Ishihara, T. and Hibi, K. (1998), "Turbulent measurements of the flow field around a high-rise building", *J. of Wind Eng.*, Japan, No.76, 55-64 (in Japanese).

Ishihara, T., Hibi, K. and Oikawa, S. (1999), "A wind tunnel study of turbulent flow over a three-dimensional steep hill", *J. Wind Eng. Ind. Aerod.*, **83**, 95-107.

Kato, M. and Launder, B. E. (1993), "The modeling of turbulent flow around stationary and vibrating square cylinders", Prep. of 9th Symp. on Turbulent shear flow, 10-4-1-6.

Kataoka, H. and Mizuno, M. (1999), "Numerical flow computation around 3d square cylinder using inflow turbulence", *J. Archit. Plann. Environ. Eng.,* AIJ, No.523,71-77 (in Japanaese).

Launder, B. E., Reece, G. J. and Rodi, W. (1975), "Progress in the development of Reynolds stress turbulence closure", *J. Fluid Mech.*, **68**, 537-566.

Lakehal, D. and Rodi, W. (1997), "Calculation of the flow past a surface-mounted cube with two-layer turbulence models", *J. Wind Eng. Ind. Aerod.*, **67/68**, 65-78.

Murakami, S., Mochida, A. and Hayashi, Y. (1990), "Examining the k-ε model by means of a wind tunnel test and large eddy simulation of turbulence structure around a cube", *J. Wind Eng. Ind. Aerod.*, **35**, 87-100.

Murakami, S. (1993), "Comparison of various turbulence models applied to a bluff body", *J. Wind Eng. Ind. Aerod.*, **46&47**, 21-36.

Murakami, S., Mochida, A. and Ooka, R. (1993), "Numerical simulation of flowfield over surface-mounted cube with various second-moment closure models", *9th Symp. on Turbulent Shear Flow*, 13-5.

Murakami, S. and Mochida, A. (1988), "3-D numerical simulation of airflow around a cubic model by means of the k-ε model", *J. Wind Eng. Ind. Aerod.*, **31**, 283-303.

Murakami, S., Mochida, A. and Hayashi, Y. (1990), "Examining the k-ε model by means of a wind tunnel test and large-eddy simulation of turbulence structure around a cube", *J. Wind Eng. Ind. Aerod.,* **35**, 87-100.

Tominaga, Y. and Mochida, A. (1999), "CFD prediction of flowfield and snowdrift around building complex in snowy region", *J. Wind. Engg. Ind. Aerod.*, **81**, 273-282.

Tsuchiya, M., Murakami, S., Mochida, A., Kondo, K. and Ishida, Y. (1997), "Development of a new k-ε model for flow and pressure fields around bluff body", *J. Wind Eng. Ind. Aerod.*, **67/68**, 169-182.

Yakhot, V. and Orszag, S. A, (1986), "Renormalization group analysis of turbulence", *J. Sci. Comput.* **1**, 3.

Yoshie, R. (1999), "CFD analysis of flow field around a high-rise building", Summaries of Technical Papers of Annual Meeting, Environ. Engg. II, AIJ (in Japanese).

Appendix 1. Outline of the revised *k-ε* models

It is well known that applications of the standard k-ε to flowfield around bluff bodies, often yield serious errors such as overestimation of k in the impinging region (Murakami *et al*. 1990, Murakami 1993). Launder and Kato (1993) proposed a revised k-ε model (hereafter denoted as LK model) which resolves the problem concerning the overestimation of k by modifying the expression of P_k as follows.

$$P_k = v_t S\Omega \tag{7}$$

$$v_t = C_\mu k^2 / \varepsilon \tag{8}$$

$$S = \sqrt{\frac{1}{2}\left(\frac{\partial U_i}{\partial x_j} + \frac{\partial U_j}{\partial x_i}\right)^2} \tag{9}$$

$$\Omega = \sqrt{\frac{1}{2}\left(\frac{\partial U_i}{\partial x_j} - \frac{\partial U_j}{\partial x_i}\right)^2} \tag{10}$$

However, this model has two points requiring revision. In the flowfield where $\Omega/S > 1$, the expression for P_k in Eq. (7) overestimates P_k compared to that for the standard k-ε model. To avoid this overestimation, Eq. (7) must be utilized only in the region where $\Omega/S < 1$. The present authors call this modification "modified LK model" (Tominaga and Mochida 1999).

Another problem of the LK model is a mathematical inconsistency in the modeling of Reynolds stress $-\langle u'_i u'_j \rangle$ and P_k (Tsuchiya *et al.* 1997). The authors' group proposed a new revision of the k-ε model, i.e., MMK model, which corrected this inconsistency of the LK model by adding the modification not to the expression for P_k but to the expression for eddy viscosity v_t.

$$v_t = C_\mu^* k^2 / \varepsilon, \ C_\mu^* = C_\mu \Omega / S \qquad (\Omega/S < 1) \tag{11}$$

$$v_t = C_\mu^* k^2 / \varepsilon, \ C_\mu^* = C_\mu \qquad (\Omega/S \geq 1) \tag{12}$$

$$P_k = v_t S^2 \tag{13}$$

LK, modified LK and MMK were used in LK1~3 and MMK1, 2. In DBN, a revised k-ε model proposed by Durbin (1996) was adopted. In this model, the eddy viscosity v_t is defined as follows.

$$v_t = C_\mu kT \tag{14}$$

T in Eq. (14) is the turbulent time scale. Durbin proposed Eq. (15) for T based on the 'realizability' constraint.

$$T = \frac{k}{\varepsilon}\min\left(1, \frac{1}{C_\mu \sqrt{3}}\frac{1}{\eta}\right) \tag{15}$$

$$\eta = \frac{Sk}{\varepsilon} \tag{16}$$

The computation based on the RNG k-ε model proposed by Yakhot and Orszag (Yakhot and Orszag 1986) was also carried out in RNG1, 2.

Appendix 2 : Models used in the DSM (Murakami *et al.* 1993)

In DSM, the commonly adopted form proposed by Launder *et al.* (1975) was used except for wall reflection term. For the wall reflection term, a model proposed by Craft and Launder (1992) was utilized.

Notation

x_i	: three components of spatial coordinate ($i = 1$; streamwise(x), $i = 2$; lateral(y), $i = 3$; vertical(z)
u_i	: velocity component in the x_i direction ($i = 1$; streamwise(u), $i = 2$; lateral(v), $i = 3$; vertical(w))
H	: height of building model
b	: width of building model
U_o	: <u> value at inflow of computational domain at height H
k	: turbulence kinetic energy
P_k	: production term of k
v_t	: eddy viscosity

ε : turbulence dissipation rate
u^* : friction velocity
$<u_i>_p$: tangential velocity component at 1st grid adjacent to solid wall
h_p : grid spacing of 1st grid adjacent to solid wall
k_p : k value at 1st grid adjacent to solis wall
z_0 : roughness parameter
τ_w : wall shear stress